Ocean Modelling 188 (2024) 102305

Contents lists available at ScienceDirect

Ocean Modelling

journal homepage: www.elsevier.com/locate/ocemod

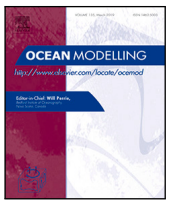

Evolution of wave directional properties in sea ice

Alberto Alberello [a,*], Emilian I. Părău [a], Qingxiang Liu [b,c], Francesca De Santi [d]

[a] School of Mathematics, University of East Anglia, Norwich, NR4 7TJ, United Kingdom
[b] Frontier Science Center for Deep Ocean Multispheres and Earth System (FDOMES) & Physical Oceanography Laboratory, Ocean University of China, Qingdao, China
[c] Department of Infrastructure Engineering, The University of Melbourne, Melbourne, 3010, Australia
[d] IMATI, Consiglio Nazionale delle Ricerche, Milano, 20133, Italy

ARTICLE INFO

Keywords:
Marginal ice zone
Waves
Directionality
Sea ice

ABSTRACT

Ocean waves and sea ice properties are intimately linked in the marginal ice zone (MIZ), nevertheless a definitive modelling paradigm for the wave attenuation in the MIZ is missing. The evolution of wave directional properties in the MIZ is a proxy for the main attenuation mechanism but paucity of measurements and disagreement between them contributed to current uncertainty. Here we provide an analytical evidence that viscous attenuation tilts the mean wave direction orthogonal to the sea ice edge and the narrows directionality. Departure from this behaviour are attributed to bimodality of the spectrum. We also highlight the need for high quality directional measurements to reduce uncertainty in the definition of the attenuation rate.

1. Introduction

Antarctic sea ice controls the fluxes of heat and momentum between the upper ocean and the lower atmosphere (Hansen et al., 2005; Andrews et al., 2009; Parkinson, 2019) and, therefore, it is a key component of Earth's climate system. Antarctic sea ice is also one of the largest and most dynamic ecosystems on Earth, its extent undergoes a dramatic seasonal cycle of melting and freezing, i.e. from less than 2 million km^2 to almost 20 million km^2. Over the past 50 years, Antarctic sea ice extent has shown no significant trend, but the observed rapid decline that began in 2016 (equivalent to 30 years of sea ice loss in the Arctic; Eayrs et al., 2021) and the recent record lows in Antarctic sea ice in 2023 suggest a future regime shift.

Coupled atmosphere–ocean–sea ice interactions that drive the advance and retreat of Antarctic sea ice are enhanced in the outer part of the seasonal sea ice zone (Massom and Stammerjohn, 2010; Alberello et al., 2020; Thomson, 2022; Elvidge et al., 2023; Tersigni et al., 2023), known as the marginal ice zone (MIZ). The MIZ is hundreds of kilometres wide (Vichi, 2022; Brouwer et al., 2022) and appears as a heterogeneous field of thin and small ice floes (Massom and Stammerjohn, 2010; Alberello et al., 2019). The most prominent feature of the MIZ is the presence of surface waves propagating from the open ocean and attenuating further into the sea ice.

Wave evolution and ice properties are intimately coupled in the MIZ (Kohout et al., 2014; Bennetts et al., 2017; Bateson et al., 2022; Alberello et al., 2022), therefore ocean waves can influence atmosphere–ocean–ice heat and momentum exchanges (Swart et al., 2019; Roach et al., 2019; Landwehr et al., 2021; Thomson, 2022). In particular, waves properties regulate the floe size distribution (Shen et al., 2004; Mokus and Montiel, 2022) that, in turn, affects wave attenuation (Squire, 2020). Nevertheless, the exact contribution of wave-induced processes to the MIZ evolution remains uncertain due to the scarcity of observations and disagreement between models (Bennetts et al., 2022).

Wave attenuation is determined by the characteristic dimension of the sea ice floes (Squire, 2020). For large floes, tens to hundreds of metres, scattering, diffraction and bending deformation are the dominant mechanisms (Masson and LeBlond, 1989; Bennetts and Squire, 2012). For small floes, more typical in the exterior of the MIZ, viscous effects and collisions are the main mechanisms. In this latter regime sea ice is modelled as an effective or homogenised layer (Keller, 1998; De Santi and Olla, 2017; Alberello and Părău, 2022; Alberello et al., 2023, individual floes not resolved). Despite a clear theoretical framework exists, experimental efforts to characterise wave attenuation in the field over the last three decades (Squire et al., 1995; Squire, 2007, 2020, for a comprehensive review) failed to provide a strong support for a definitive modelling paradigm. This is exemplified by the variety of parameterisations available in WAVEWATCH III, i.e. the state-of-the-art spectral wave model.

The wave directional properties in sea ice can be a diagnostic of the dominant attenuation mechanism (Sutherland and Gascard, 2016; Wahlgren et al., 2023). Scattering broadens of the wave spectrum while

* Corresponding author.
E-mail address: A.Alberello@uea.ac.uk (A. Alberello).

https://doi.org/10.1016/j.ocemod.2023.102305
Received 28 October 2023; Received in revised form 13 December 2023; Accepted 15 December 2023
Available online 20 December 2023

viscous-like effect narrow it. In both cases the mean wave direction turns orthogonal to the sea ice edge due to the path-length effect, i.e. a component at an angle has to travel a longer distance over ice and is therefore subjected to higher attenuation. Neither of the two mechanisms affects the dispersion relation (Meylan et al., 2018) (supported by measurements for waves longer than 5 s; Cheng et al., 2017; Collins et al., 2018) and therefore changes the direction, similar to refraction.

Direct observations of directional wave properties in sea ice are challenging (Gemmrich et al., 2021) and measurements of directional spread have been contradictory, whereas they generally agree that the mean wave direction turns orthogonal to the ice edge during propagation. Early field experiments, based on wave buoys, showed both narrowing (Squire and Moore, 1980) and broadening (Wadhams et al., 1986; Meylan et al., 1997) up to isotropy. More recent measurements by Sutherland & Gacard (Sutherland and Gascard, 2016), with airborne LiDAR, reported an increase of directionality, particularly for short wave components (at the spectral peak the spread remains unchanged) where scattering is predicted to be more important. Overall, most authors reported narrowing using wave buoys (Montiel et al., 2018), SAR (Ardhuin et al., 2020) and shipborne stereo-imaging (Alberello et al., 2022), particularly for long wave components (Ardhuin et al., 2016).

The analysis of the directional properties measured in the field is made challenging by the complex directional structure of ocean wave spectra where swell and wind waves coexist, each propagating in its own direction. Bimodality of ocean wave spectra in the field can therefore lead to uncertainty during interpretation of field measurements (e.g. Alberello et al., 2022). This issue affects the most the widely used wave buoys that only transmit spectral moments (Longuet-Higgins, 1963; Kuik et al., 1988). These integrated quantities tend to smooth variability required to precisely separate directional features.

To understand the evolution of directional wave spectra in sea ice, an analytical model is proposed. The focus is the Southern Ocean and Antarctic MIZ where waves are hundred metres long (Derkani et al., 2021a) and floes are small (< 10 m; Alberello et al., 2019). In this regime viscous-like attenuation is the main attenuation mechanism. This paper provides a detailed analysis of the effect of sea ice dissipation on directional wave properties. Here we analyse the evolution of unidirectional and directional (unimodal and bimodal) synthetic wave fields. Implications for the evolution of measured Southern Ocean sea states are also discussed.

2. Sea ice attenuation

In sea ice, the wave amplitude is attenuated as a function of the propagation distance. To reduce the problem to one dimension in the direction normal to the ice edge (x), an infinite sea-ice edge aligned along the y axis with a homogeneous incident wave field is assumed. This simplified setup is representative of the Antarctic MIZ, where the sea ice edge is oriented in the zonal direction (latitude line; y-axis) and waves propagate towards Southern sectors (along the positive x-axis).

Wave energy is attenuated exponentially in sea ice, and at a frequency-dependent rate, i.e. high frequency components are subject to greater attenuation (Wadhams et al., 1988). Each component of the frequency-direction spectrum ($S(f,\theta)$; where f is the frequency and θ is the direction of the angle of incidence relative to the normal) at a distance (x) from the ice edge is obtained as:

$$S(f,\theta;x) = S(f,\theta;0)\exp\left(\frac{-\int_0^x \alpha(f;s)ds}{cos\theta}\right). \tag{1}$$

$S(f,\theta;0)$ denotes the incident spectrum (at the sea ice edge) and α the attenuation rate. The term $(\cos\theta)^{-1}$ accounts for the path-length effect, i.e. the greater distance that the wave components that propagate at an angle to the ice edge have to travel. Eq. (1) is derived from geometrical argument.

The attenuation rate is proportional to physical properties of the sea ice cover (e.g. thickness, stiffness, concentration) and therefore can vary in space. For simplicity, it is assumed that α is constant in x, i.e. $\alpha(f;x) = \alpha(f)$, therefore Eq. (1) can be written as:

$$S(f,\theta;x) = S(f,\theta;0)\exp\left(\frac{-\alpha(f)x}{cos\theta}\right). \tag{2}$$

Different wave attenuation models, under assumptions of deep water and small attenuation, all lead to a power-law relationship (De Santi et al., 2018). Among these, without loss of generality, the empirical power law polynomial from (Meylan et al., 2014) is assumed:

$$\alpha(f) = Af^2 + Bf^4, \tag{3}$$

with parameters $A = 2.12\times10^{-3}$ s^2 m^{-1} and $B = 4.59\times10^{-2}$ s^4 m^{-1}.

In addition to the frequency-direction spectrum, some integral parameters will be tracked: significant wave height (H_S), mean wave period (T_m), mean wave direction (θ_1) and directional spreading (σ_1). These are defined as:

$$H_S = 4\sqrt{m_0}, \tag{4}$$

$$T_m = \frac{m_{-1}}{m_0}, \tag{5}$$

$$\theta_1 = \arctan\left(\frac{b_1}{a_1}\right), \tag{6}$$

$$\sigma_1 = \sqrt{2\left(1-\sqrt{a_1^2+b_1^2}\right)}. \tag{7}$$

In Eqs. (4)–(6) the nth order moments are:

$$m_n = \int_{-\pi/2}^{\pi/2}\int_0^\infty f^n S(f,\theta)df\,d\theta, \tag{8}$$

and the angular moments:

$$a_1 = \int_0^\infty\int_{-\pi/2}^{\pi/2}\cos\theta S(f,\theta)d\theta df, \tag{9}$$

$$b_1 = \int_0^\infty\int_{-\pi/2}^{\pi/2}\sin\theta S(f,\theta)d\theta df. \tag{10}$$

It should be noted that the integration is carried out only for the wave components that propagate in the positive directions, i.e. in the sector between $-\pi/2$ and $+\pi/2$. Possible propagation of waves from the MIZ to the open ocean is not taken into account.

3. Unidirectional wave field

The spatial evolution of a unidirectional wave spectrum is analysed considering three different angles of incidence (0°, 30°, and 60°). Without loss of generality, a Pierson–Moskowitz (PM) spectrum is used:

$$S(f;0) = \frac{ag^2}{(2\pi f)^5}\exp\left(-b\frac{f_0^4}{f^4}\right) \tag{11}$$

with coefficients $a = 8.1\times10^{-3}$ and $b = 0.74$. Here $f_0 = f_p/0.877$, where f_p is the peak wave frequency, i.e. the spectral component with the highest energy.

Fig. 1 shows the spatial evolution of the significant height (Fig. 1a) and mean wave period (Fig. 1b), both normalised with respect to their counterparts at the ice edge, for a spectrum with $f_0 = 0.1$ Hz. We assume that dissipation is constant over a distance of 100 km to highlight the effect of viscous dissipation on wave propagation. In the field, attenuation is expected to vary over this lengthscale due to the changing morphology of sea ice and Eq. (1) should be preferred for applications. We note, however, that detailed information about the spatial variability of α are seldom available. The wave height is reduced during propagation in sea ice in all cases but the attenuation rate is greater for larger angles of incidence. This result reflects the longer

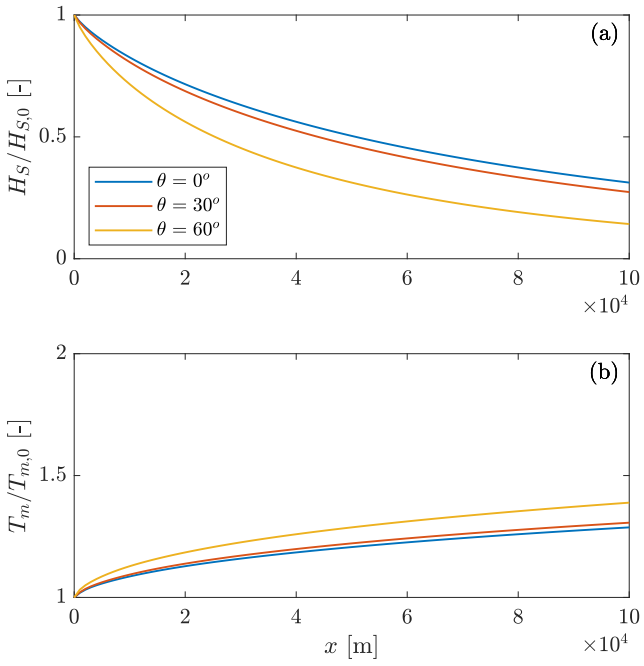

Fig. 1. Normalised wave height (a) and mean wave period (b) of a PM spectrum with $f_0 = 0.1$ Hz as a function of distance from the ice edge for varying angle of incidence.

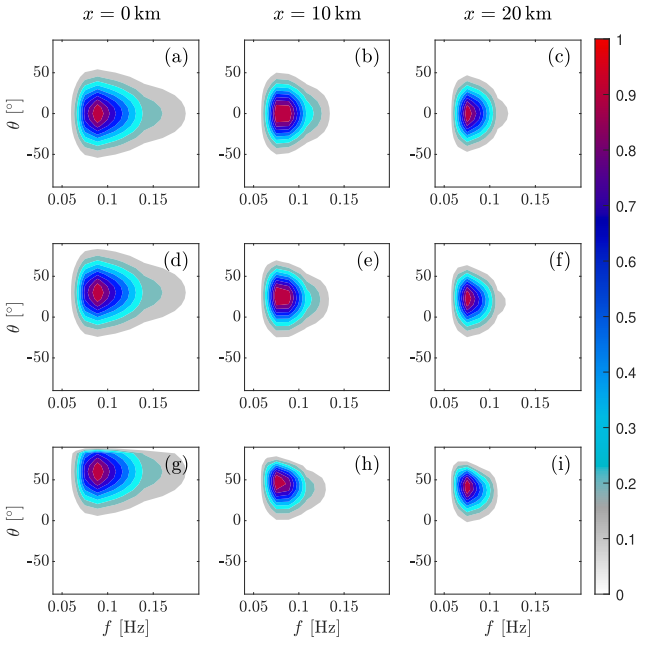

Fig. 2. Spatial evolution of the 2d wave spectrum in sea ice at distance 0 km (a,d,g), 10 km (b,e,h) and 20 km (c,f,i) for the three incidence angles of 0° (a–c), 30° (d–f) and 60° (g–i). Directional spread $N = 20$. Each spectrum is normalised by its maximum value.

distance that waves at an angle have travelled in the ice, see Eq. (2). The difference in attenuation rate is proportional to $(\cos\theta)^{-1}$, so a wave obliquely incident on the ice edge is equivalent to a shorter wave normally incident. For example, a 10 s wave with a 60° (30°) angle of incidence is equivalent to a ≈7.5 s component (≈9.4 s) normal to the ice edge for the attenuation rate defined by Eq. (3).

Fig. 1b demonstrates the increase of the mean wave period during wave propagation in sea ice. This is a consequence of the differential attenuation rate across spectral components (e.g. Alberello and Părău, 2022). Changes in mean wave period are more significant for waves at an angle with respect to the sea ice edge, also due to the longer distances have to transit over sea ice compared to waves approaching at a normal angle.

4. Directional wave field

4.1. Unimodal sea state

Here we assign a directional distribution to the 1D spectrum analysed in the previous Section 3, assuming that the directionality is frequency independent, i.e. $S(f,\theta) = D(\theta)S(f)$. The directional distribution $D(\theta) = d_N \cos^N(\theta/2 - \theta_0/2)$ is used (Goda, 1999), where d_N is a normalisation factor (such as $\int_{-\pi/2}^{+\pi/2} D d\theta = 1$) and N is the spreading parameter. Large N produce narrow seas (e.g. swells; $N = \infty$ corresponds to a unidirectional field) and small N produce broad seas (e.g. young wind-forced seas).

The spatial evolution of waves with three different values of directional spread ($N = 1$, 20, 100) is examined for the same three mean wave direction of Section 3.

The effect of dissipation at 3 distances from the sea ice edge (0, 10 and 20 km) for the intermediate value of directional spread ($N = 20$) and the three incidence angles is illustrated in Fig. 2. Spectra are all normalised by their respective maximum to highlight changes in the shape of the spectrum.

The spectrum with mean wave direction 0° (Fig. 2a–c) remains symmetric with respect to the radial coordinate in ice. However, it becomes narrower due to stronger dissipation for waves propagating at an angle. For spectra with the mean wave direction at an angle to the normal (Fig. 2d–f and g–i) the differential attenuation causes the peak to rotate closer to the normal. Due to the lower attenuation of the component propagating along the normal, i.e. $\theta = 0$, this becomes dominant at large x. These spectra also lose their initial symmetry in the radial direction.

A quantitative analysis of all integrated spectral parameters for N and angles of incidence is shown in Fig. 3. For broad directional spectra and high angles of incidence, some of the energy propagates towards the open ocean, i.e. away from the ice. These components are not included in the integrated parameters that only account for the forward propagating part of the spectrum (they are defined by integrating within the sector $-\pi/2$ to $+\pi/2$). In the cases in which energy propagates away from the ice, for completeness, the values of the full spectral parameters (i.e. integrated over 360°) are indicated in Fig. 3 with asterisks.

The evolution of H_S and T_m for narrow directional spreading ($N = 100$; Fig. 3c–f) is similar to that of the 1D spectrum for all angles of incidence. The energy in the ice is higher for the mean wave direction 0°, as the majority of the wave energy is propagating in the nearly normal directions. Conversely, when the spectrum is broad, i.e. $N = 1$ (Fig. 3a–d), the difference between the different angles of incidence disappears. Wave energy is more evenly distributed in directions and the path-length effect becomes more important than the initial angle of incidence.

The mean wave direction (Fig. 3g–i) is reduced by propagation in sea ice, i.e. waves tend to turn towards the normal angle of incidence, and directionally spread sea states turn faster. The directional spread also reduces during wave propagation in sea ice (Fig. 3j–l). The decrease is stronger for more directionally spread waves, whereas narrow spectra undergo little change.

4.2. Bimodal sea state

Sea states in the ocean are often bimodal. Wind sea and swell coexist and have different mean directions of propagation, i.e. crossing seas. Here a swell with $f_0 = 0.09$ Hz and a wind sea with $f_0 = 0.11$ Hz are

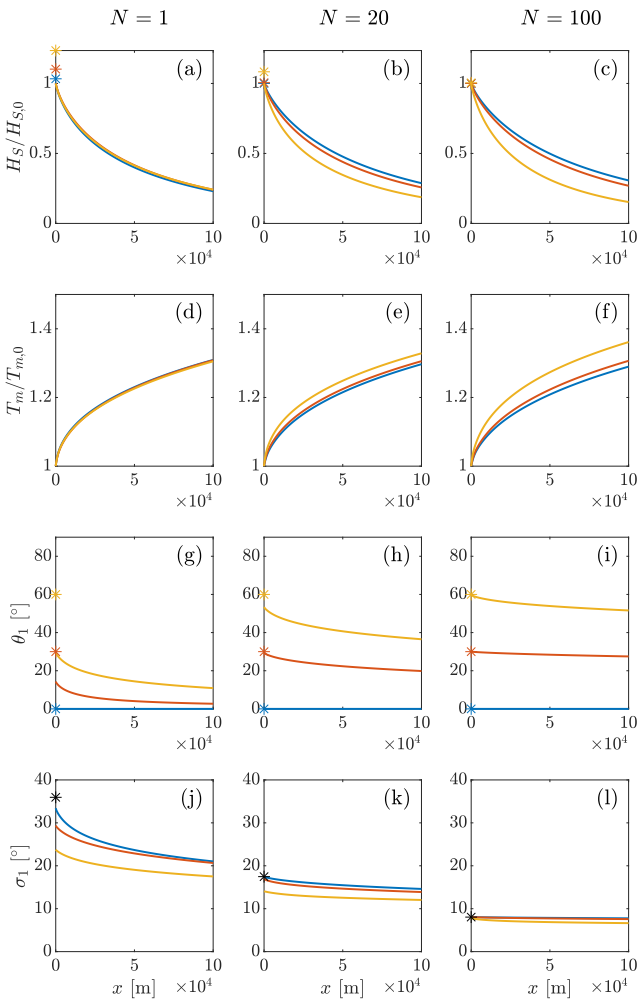

Fig. 3. Integrated spectral parameters of a PM spectrum with $f_0 = 0.1$ Hz as a function of distance from the ice edge and the normal angle of incidence for $N = 1$, 20, 100. Each line denotes a different angle of incidence, colour-coded as in Fig. 1a Where presents, asterisks denote the full spectrum (integrated over 360°). Note that directional spreading of the full spectrum is unaffected by angle of incidence (black asterisk).

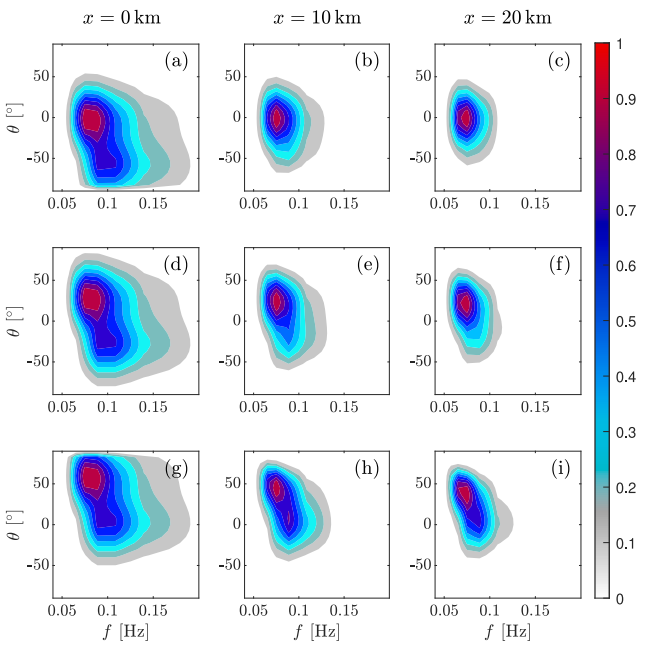

Fig. 4. Directional wave spectra for a crossing sea at the ice edge ($x = 0$ m) and in sea ice ($x = 5 \times 10^4$ m and $x = 10 \times 10^4$ m) for the three incidence angles of the swell of 0°, 30° and 60°. Each spectrum is normalised by its maximum value.

considered. The swell and wind sea are assigned a mean wave direction 60° from each other. The mean swell directions are 0°, 30° and 60° (and the corresponding wind seas −60°, −30° and 0°, respectively). Both energy distributions are defined by a PM, but the swell coefficient a is reduced by a factor of 4 to give similar energy for both wave systems. The same directional spread is assigned to both sea states ($N = 20$). Each wave component is propagated according to linear wave theory for which linear superposition is valid (wave–wave nonlinear interaction are suppressed). The assigned energy and directional spread are unlikely in the field, actual measured Southern Ocean wave spectra will be examined in Section 5.

The spectral evolution at different distances from the ice edge is shown in Fig. 4. When the swell is normal and the wind sea is oblique (Fig. 4a–c), the wind sea dissipates rapidly, leaving only the component associated with the swell. The spectrum tends to become more symmetric. When the wind sea and the swell are both obliquely incident (Fig. 4d–f), the spectrum remains elongated in the radial direction, with the peak rotating in the direction normal to the sea ice edge. Both spectra are similarly attenuated. However, the swell is more energy-conserving because its peak is at a lower and less dissipative frequency. When the wind sea is normal and the swell is angular (Fig. 4g–i), the lower dissipation at 0° compensates for the shorter period of the wind sea compared to the swell. As a result, at 50 km (Fig. 4h) the peak associated with the wind sea is preserved. At 100 km (Fig. 4i) the spectrum appears to be unimodal, but stretched radially towards the original wind sea direction.

The spatial evolution of the directionally integrated spectrum is shown in Fig. 5. When the swell is along the 0° direction (Fig. 5a), the wind sea dissipates rapidly. Farther in the ice edge, the total sea state almost coincides with the swell. On the other hand, when the wind sea is in the 0° direction, the larger distance that the swell has to travel leads to a larger relative dissipation (Fig. 5c). As a result, the two systems preserve a similar amount of energy. An intermediate behaviour occurs when both wind sea and swell are at an angle to the normal direction (Fig. 5b). In all cases, propagation in sea ice leads to a downshifted of the peak and great attenuation in the high-frequency tail of the spectrum.

The spatial evolution of the frequency integrated spectrum, i.e. the directional distribution, is shown in Fig. 6. Similar to the directionally integrated spectrum, in the case of an oblique wind sea, this system dissipates rapidly and the swell contributes the most to the total (Fig. 6a). An almost symmetric distribution corresponding to the swell alone is observed further away from the ice edge. On the other hand, when the swell is oblique (Fig. 6c), the resulting spectrum is an average of the two systems. In the ice, the directional distribution appears as an unimodal system, but with an elongated tail in the direction of the wind sea. An intermediate behaviour is observed when both components are at an angle (Fig. 6b). In all cases, the initial directional distribution (dashed line in Fig. 6) is narrowed.

The spatial evolution of the integrated spectral parameter is shown in Fig. 7. The dissipation is similar in all cases (the energy is slightly lower when the swell is oblique, Fig. 7c), but for a normally incident swell the contribution of the wind sea is minimal, whereas for a normal wind sea their contribution is similar. The mean wave period of the total sea increases (Fig. 7), slightly more when the wind sea is along the 0°. The change in mean wave period of the wind sea and swell is similar in all cases. Individually, both wind sea and swell tend to align with the normal direction (Fig. 7g–i). When both wind sea and swell are oblique, the mean wave direction of the whole sea, initially aligned with the normal direction, deviates towards the more energetic swell

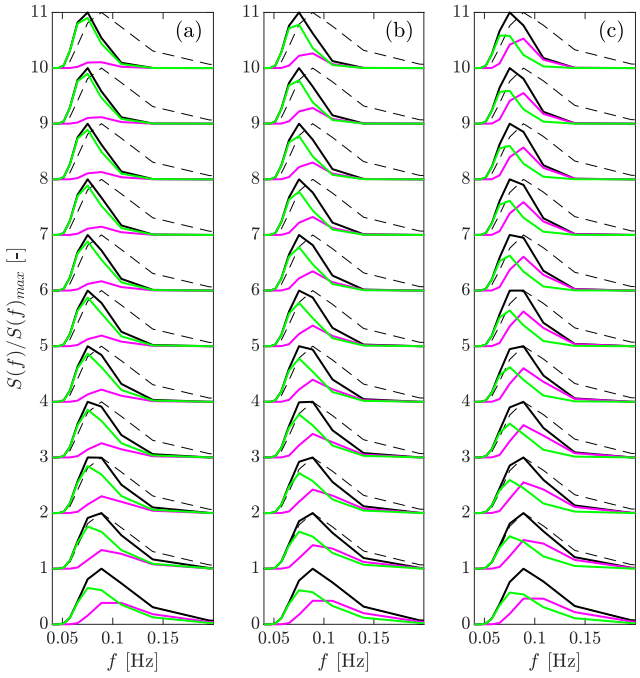

Fig. 5. Normalised frequency spectra for a crossing sea (black) plotted every 10 km. The contribution of the swell (green) and the wind sea (magenta) is also shown. Dashed black line denotes normalised frequency spectra at the $x = 0$ to better highlight its change (solid black line).

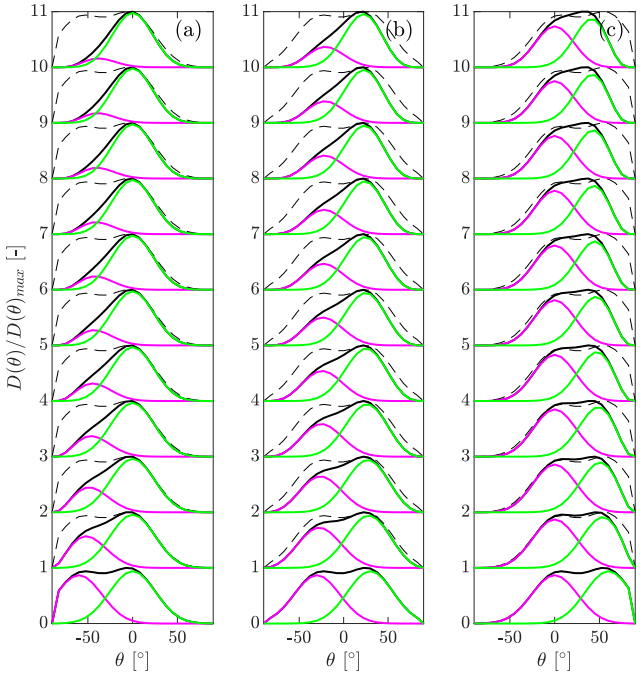

Fig. 6. Normalised directional distribution for a crossing sea (black) plotted every 10 km. The contribution of the swell (green) and the wind sea (magenta) is also shown. Dashed black line denotes normalised directional distribution at the $x = 0$ to better highlight its change (black solid line).

system (Fig. 7h). This deviation is caused by the complex structure of the bimodal sea state. The mean directional spread is reduced for all components and for the whole sea (Fig. 7g–i) in all cases, however the mean directional spread of the whole sea decreases more when the swell is along the normal direction. The component with the largest

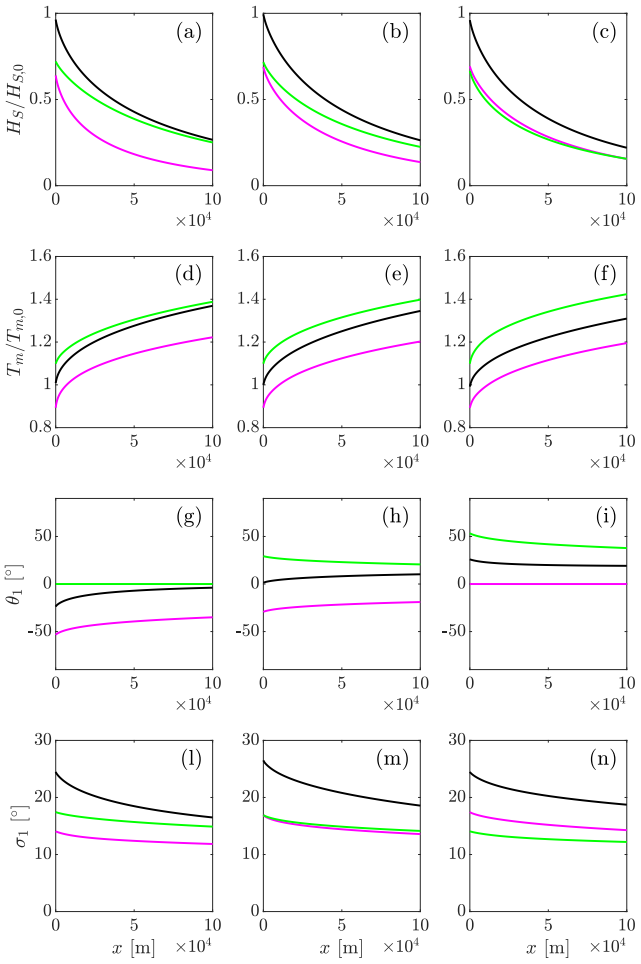

Fig. 7. Integrated spectral parameters of a crossing sea (black) with wind sea peak period of 9 s (magenta) and swell peak period 11 s (green) as a function of distance from the ice edge. Wind sea and swell have a 60° difference, and the swell normal angle of incidence is 0°, 30°, and 60°.

spread is the one closer to 0°. This is expected from the analysis of the unimodal sea state (see Fig. 3).

5. Southern ocean waves

The spatial evolution of Southern Ocean spectra measured near the sea ice edge during the Antarctic Circumnavigation Expedition (ACE; Landwehr et al., 2021; Derkani et al., 2021a) is studied in this section. The acquisition system and processing pipeline were based on the WaMoS–II system described in Derkani et al. (2021a), and quality controlled 2D frequency-direction spectra are provided (Alberello et al., 2021; Derkani et al., 2021b). The WaMoS–II system is not designed for acquisition in sea ice. The ACE dataset is used because is one of the few, to the best of our knowledge, that provides full 2D spectra in the Southern Ocean in proximity of the sea ice edge, and for a wide range of representative wave conditions.

The analysis is limited to measurements collected during Leg 2 of ACE, in the Pacific Ocean sector, when the expedition was closest to the sea ice edge and South of 60°S. This limits the analysis to two periods, 7–11 and 16–19 February 2017.

Wave spectra are evolved in space only accounting for sea ice dissipation, other possible source terms (wind input, nonlinear energy transfer, wave breaking) are suppressed in this idealised setup. The predicted evolution of three randomly selected spectra is shown in Fig. 8. The sea ice edge is assumed to be in an east–west direction.

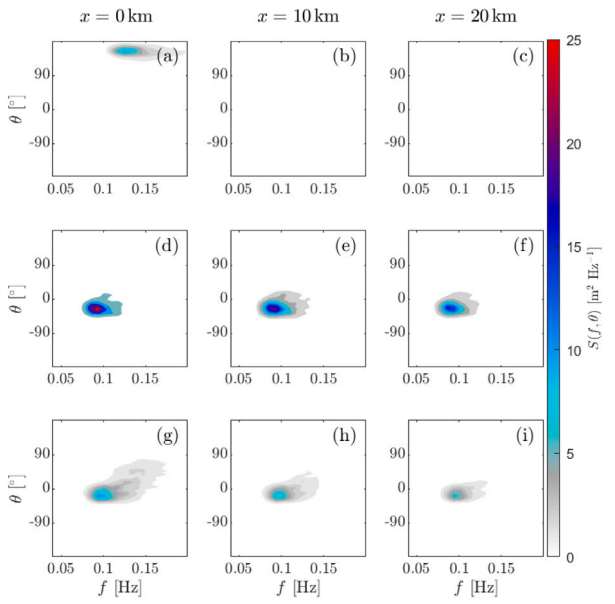

Fig. 8. Measured Southern Ocean wave spectra during ACE and their predicted evolution at 10 km and 20 km.

The first spectrum propagates mostly to the north and away from the sea ice edge (Fig. 8a). As a result, no energy is propagated to the south. In the second case (Fig. 8d) the spectrum appears unimodal with its peak close to −20°. Although not symmetrical, this case is similar to the analytical unimodal 2D spectrum propagating at an angle (cf. Fig. 2d–f). A rotation of the peak towards the normal direction can be observed. In the third case (Fig. 8g), the spectrum is bimodal, but the peak associated with the swell is much larger than the wind sea. Also, the swell system at $f \approx 0.10$ Hz is close to −10° (south-east) and the wind sea at $f \approx 0.15$ Hz propagates at ≈ 50° (south-west). The wind sea is rapidly dissipated during propagation in ice and the swell rotates to the south.

To highlight the effect of directionality, we compare the results obtained using 1D and 2D models.

1. The 1D model considers the spectrum integrated over all directions, i.e. $S(f)$, and with all components propagating along the mean wave direction.
2. The 2D model considers the full 2D spectrum, $S(f, \theta)$. In this case, each directional component is propagated along its direction.

Note that the 1D model reproduces a wide variety of available field measurements in which $S(f)$ is available but details about directional spreading are limited or missing.

In Fig. 9a we show the wave height measured at the sea ice edge and the one predicted after 50 km of propagation in ice. For the 1D simulations, the spectrum measured at the edge is shown in dark blue. When the mean wave direction is towards the Northern sectors (away from the ice), the resulting wave height at 50 km is not shown. In all other cases (mean wave direction towards south), a strong reduction of the wave height is observed (shown in light blue). For the 2D simulations, the spectrum measured at the edge is only integrated over the southern sector (in black), resulting in a lower wave height compared to the 1D counterpart, up to 50% less. The resulting wave height in the ice is reduced (magenta), but in most cases it is greater than or equal to that predicted by the 1D model. In the most extreme cases, there is a 2 m difference at 50 km between the 1D and 2D models.

The effect of the 1D and 2D models is dramatic on the mean wave period, see Fig. 9b. During the observed interval, the southward components have a mean wave period of ≈ 10s (in black). The 1D spectrum

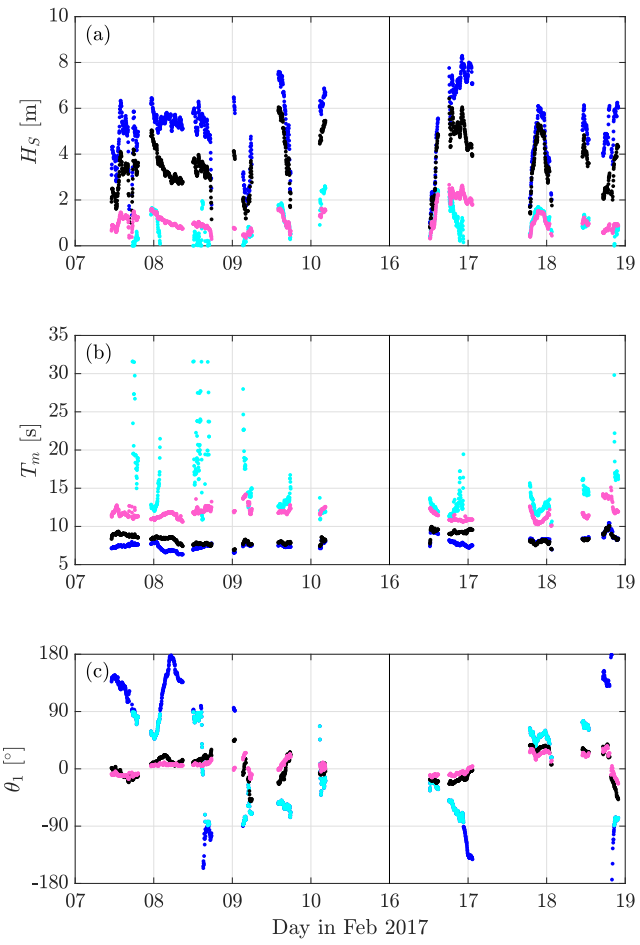

Fig. 9. Wave properties measured during ACE and their predicted value 50 km from the ice edge for (a) significant wave height, (b) mean wave period, and (c) mean wave direction. Incident wave properties in dark blue and incident wave properties of the Southward component in black. Results from 1D model in light blue, and for the 2D model in magenta.

(in dark blue) has a shorter mean wave period, ≈ 8 s in most cases. The 2D model predicts a lengthening of the mean wave period, periods of 10–15 s, but the 1D model predicts significantly longer mean wave periods, up to 35 s (note that these periods are beyond the capabilities of traditional wave buoys, and they are considered infragravity waves).

The mean wave direction in the 1D model does not change during propagation in sea ice (see Fig. 9c). In the 2D model, the mean wave direction of the forward propagating part of the spectrum is comprised in the ±30° band and during propagation it generally turns towards the 0° direction, as observed for the synthetic spectra analysed in previous sections.

The wave directional properties have dramatic implications on the estimation of the attenuation rate, see Fig. 10a. The overall attenuation rate between the sea ice edge and a point at $d_{50} = 50$ km is defined as

$$\beta = \frac{1}{d_{50}} \log \frac{H_{S,0}}{H_{S,50}}. \tag{12}$$

While for the 2D model β remains in the 2–4×10^{-5} m^{-1} range, the 1D model predicts a far large variability, exceeding 15×10^{-5} m^{-1}. Differences are most noticeable when the mean wave direction is at high angles with respect to the ice edge. Our analysis demonstrates that this variability is due to a poor representation of the directional features of the spectrum. Similarly, the downshift of the mean wave period is confined to ≈ 1.5 in the 2D model (Fig. 10b), but the 1D model would predict a significantly greater downshift rate.

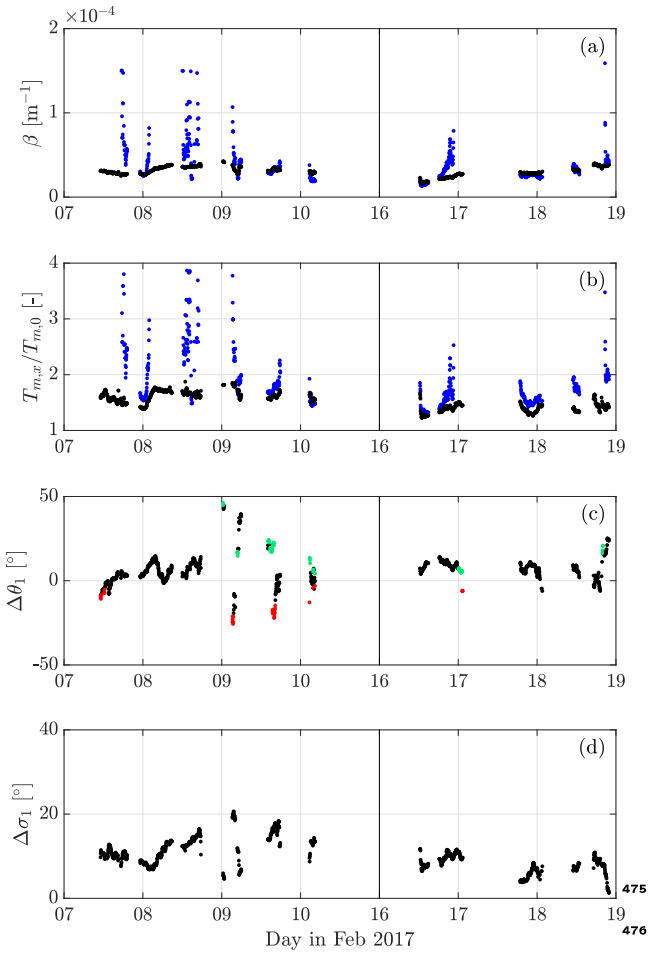

Fig. 10. Predicted attenuation rate (a), downshift (b), change in direction (c) and, directional spread (d). Results from 1D model in blue, and for the 2D model in black In (c) green dots denote a turn that takes to South but on the opposite direction, and red dots cases in which the angle after transformation is greater.

In the 2D model, in the majority of cases (> 90%) the mean wave direction rotates towards the normal direction (black dots in Fig. 10c), by up to 45°. There are instances where the mean wave direction rotates in the opposite direction with respect to the initial angle (i.e. south-west to south-east or vice-versa). These are denoted in green when the initial angle is greater than the one in ice and in red otherwise. These latter cases occur when the mean wave direction of the whole sea is close to ±90° and corresponds to < 5% of the instances. The results therefore confirm that viscous dissipation would cause the waves to turn in the normal direction of incidence, although some exceptions may occur for certain directional configurations of the sea state. On the other hand, the directional propagation of the southward component always tends to narrow (Fig. 10d), and over 50 km the narrowing is in the range of 5°–20°, with an average of ≈ 10°.

6. Summary

We investigated analytically the evolution of wave properties in the MIZ assuming that viscosity is the only attenuation mechanism. In this regime, the wave spectrum tilts towards the normal direction, i.e. orthogonal to the sea ice edge, and the directional spread is decreased. We demonstrated that these changes are an effect of the increased distance due to off-normal components (path-length effect). The turning of the mean wave direction is similar to refraction near the coast, but in that case is due to change in the relation whereas in our simulations the dispersion relation in ice remains unaltered (open ocean and deep water). Tilting away from the normal is possible, but only in crossing seas. The evolution of the directional properties prescribed by our simulation is in agreement with field observations (Montiel et al., 2018), therefore suggesting that viscous damping is the main attenuation mechanism in the MIZ. Our analysis demonstrates that unexpected behaviour observed in the field and wrongly attributed to different physical mechanisms is explained by sea ice viscous dissipation alone. Note that this may be different in the interior of the ice pack where the ice cover is continuous and acts as an elastic slab therefore changing the dispersion relation. An analysis for more realistic conditions (e.g. varying dissipation and complex geometry), also including other source terms, should be performed with the aid of spectral wave models to investigate the interplay of sea ice dissipation and other physical mechanism (e.g. nonlinear wave interactions, wind input, wave breaking) and their respective effect on the directional wave properties.

We also examined the effect of the directional spectral properties by comparing the evolution of the 2D spectrum and a corresponding 1D spectrum. The latter case replicate field measurements reported in the literature for which only partial information about the directional properties are available. For example, the analysis of wave buoy measurements is often limited to the first angular moments which smooth directional properties and, therefore, bimodality. We showed that the 2D simulations conserve more energy, resulting in a reduced attenuation coefficient, and the elongation of the mean wave period is less noticeable. Furthermore, we showed that the directional properties allow to only account for the forward propagating part of the spectrum when estimating attenuation. In contrast, in 1D simulations all energy is propagated along the mean wave direction resulting in a large variability of the derived attenuation rate.

We argue that the current paucity of directional measurements and their often contradictory outcome contributed to the uncertainty on the definition of the dominant attenuation mechanisms in the MIZ. Thus, our analysis highlights the need for high quality 2D measurements in the MIZ.

CRediT authorship contribution statement

Alberto Alberello: Conceptualization, Formal analysis, Methodology, Visualization, Writing – original draft, Writing – review & editing. **Emilian I. Părău:** Methodology, Writing – original draft, Writing – review & editing. **Qingxiang Liu:** Methodology, Writing – original draft, Writing – review & editing. **Francesca De Santi:** Methodology, Visualization, Writing – original draft, Writing – review & editing.

Declaration of competing interest

The authors declare that they have no known competing financial interests or personal relationships that could have appeared to influence the work reported in this paper.

Data availability

No data was used for the research described in the article.

Acknowledgements

AA and EP acknowledge funding from EPSRC, United Kingdom (EP/Y02012X/1). AA and FDS acknowledge support from the London Mathematical Society, United Kingdom through the Research in Pairs – Scheme 4 (Ref. 42250).

References

Alberello, Alberto, Bennetts, Luke, Heil, Petra, Eayrs, Clare, Marcello Vichi, Keith MacHutchon, Onorato, Miguel, Toffoli, Alessandro, 2020. Drift of pancake ice floes in the winter antarctic marginal ice zone during polar cyclones. J. Geophys. Res.: Oceans 125 (3), e2019JC015418.

Alberello, A., Bennetts, L.G., Onorato, M., Vichi, M., MacHutchon, K., Eayrs, C., Ntamba, B.N., Benetazzo, A., Bergamasco, F., Nelli, F., Pattani, R., Clarke, H., Tersigni, I., Toffoli, A., 2022. Three-dimensional imaging of waves and floes in the marginal ice zone during a cyclone. Nature Commun. 13 (4590), 1–11.

Alberello, A., Bennetts, L., Toffoli, A., Derkani, M., 2021, Antarctic Circumnavigation Expedition 2016-2017: Wamos Data, Australian Antarctic Data Centre.

Alberello, A., Onorato, M., Bennetts, L., Vichi, M., Eayrs, C., MacHutchon, K., Toffoli, A., 2019. Brief communication: Pancake ice floe size distribution during the winter expansion of the antarctic marginal ice zone. Cryosphere 13 (1), 41–48.

Alberello, Alberto, Parau, Emilian, Chabchoub, Amin, 2023. The dynamics of unstable waves in sea ice. Sci. Rep. 13.

Alberello, Alberto, Părău, Emilian, 2022. A dissipative nonlinear Schrödinger model for wave propagation in the marginal ice zone. Phys. Fluids 34 (6).

Andrews, Timothy, Forster, Piers M., Gregory, Jonathan M., 2009. A surface energy perspective on climate change. J. Clim. 22 (10), 2557–2570.

Ardhuin, Fabrice, Otero, Mark, Merrifield, Sophia, Grouazel, Antoine, Terrill, Eric, 2020. Ice breakup controls dissipation of wind waves across southern ocean sea ice. Geophys. Res. Lett. 47 (13), e2020GL087699.

Ardhuin, Fabrice, Sutherland, Peter, Doble, Martin, Wadhams, Peter, 2016. Ocean waves across the arctic: Attenuation due to dissipation dominates over scattering for periods longer than 19 s. Geophys. Res. Lett. 43 (11), 5775–5783.

Bateson, A.W., Feltham, D.L., Schröder, D., Wang, Y., Hwang, B., Ridley, J.K., Aksenov, Y., 2022. Sea ice floe size: its impact on pan-arctic and local ice mass and required model complexity. Cryosphere 16 (6), 2565–2593.

Bennetts, L.G., Bitz, C.M., Feltham, D.L., Kohout, A.L., Meylan, M.H., 2022. Marginal ice zone dynamics: future research perspectives and pathways. Phil. Trans. R. Soc. A 380 (2235), 20210267.

Bennetts, L.G., O'Farrell, S., Uotila, P., 2017. Brief communication: Impacts of ocean-wave-induced breakup of antarctic sea ice via thermodynamics in a stand-alone version of the cice sea-ice model. Cryosphere 11 (3), 1035–1040.

Bennetts, Luke G., Squire, Vernon A., 2012. On the calculation of an attenuation coefficient for transects of ice-covered ocean. Proc. R. Soc. A 468 (2137), 136–162.

Brouwer, J., Fraser, A.D., Murphy, D.J., Wongpan, P., Alberello, A., Kohout, A., Horvat, C., Wotherspoon, S., Massom, R.A., Cartwright, J., Williams, G.D., 2022. Altimetric observation of wave attenuation through the antarctic marginal ice zone using icesat-2. Cryosphere 16 (6), 2325–2353.

Cheng, Sukun, Erick Rogers, W., Thomson, Jim, Smith, Madison, Doble, Martin J., Wadhams, Peter, Kohout, Alison L., Lund, Björn, Persson, Ola P.G., Collins, Clarence O., Ackley, Stephen F., Montiel, Fabien, Shen, Hayley H., 2017. Calibrating a viscoelastic sea ice model for wave propagation in the arctic fall marginal ice zone. J. Geophys. Res.: Oceans 122 (11), 8770–8793.

Collins, Clarence, Doble, Martin, Lund, Björn, Smith, Madison, 2018. Observations of surface wave dispersion in the marginal ice zone. J. Geophys. Res.: Oceans 123 (5), 3336–3354.

De Santi, Francesca, De Carolis, Giacomo, Olla, Piero, Doble, Martin, Cheng, Sukun, Shen, Hayley H., Wadhams, Peter, Thomson, Jim, 2018. On the ocean wave attenuation rate in grease-pancake ice, a comparison of viscous layer propagation models with field data. J. Geophys. Res.: Oceans 123 (8), 5933–5948.

De Santi, Francesca, Olla, Piero, 2017. Effect of small floating disks on the propagation of gravity waves. Fluid Dyn. Res. 49 (2), 025512.

Derkani, M.H., Alberello, A., Nelli, F., Bennetts, L.G., Hessner, K.G., MacHutchon, K., Reichert, K., Aouf, L., Khan, S., Toffoli, A., 2021a. Wind, waves, and surface currents in the southern ocean: observations from the antarctic circumnavigation expedition. Earth Syst. Sci. Data 13 (3), 1189–1209.

Derkani, M., Alberello, S., Toffoli, A., 2021b, Antarctic circumnavigation expedition 2017: Wamos data product. Australian Antarctic Data Centre.

Eayrs, Clare, Li, Xichen, Raphael, Marilyn N., Holland, David M., 2021. Rapid decline in Antarctic sea ice in recent years hints at future change. Nat. Geosci. 14 (7), 460–464.

Elvidge, A.D., Renfrew, I.A., Edwards, J.M., Brooks, I.M., Srivastava, P., Weiss, A.I., 2023. Improved simulation of the polar atmospheric boundary layer by accounting for aerodynamic roughness in the parameterization of surface scalar exchange over sea ice. J. Adv. Modelling Earth Syst. 15 (3), e2022MS003305.

Gemmrich, Johannes, Mudge, Todd, Thomson, Jim, 2021. Long-term observations of the group structure of surface waves in ice. Ocean Dyn. 71 (3).

Goda, Yoshimi, 1999. A comparative review on the functional forms of directional wave spectrum. Coastal Eng. J. 41 (1), 1–20.

Hansen, James, Nazarenko, Larissa, Ruedy, Reto, Sato, Makiko, Willis, Josh, Del Genio, Anthony, Koch, Dorothy, Lacis, Andrew, Lo, Ken, Menon, Surabi, et al., 2005. Earth's energy imbalance: Confirmation and implications. Science 308 (5727), 1431–1435.

Keller, Joseph B., 1998. Gravity waves on ice-covered water. J. Geophys. Res.: Oceans 103 (C4), 7663–7669.

Kohout, A.L., Williams, M.J.M., Dean, S.M., Meylan, M.H., 2014. Storm-induced sea-ice breakup and the implications for ice extent. Nature 509 (7502), 604–607.

Kuik, A.J., Ph van Vledder, G., Holthuijsen, L.H., 1988. A method for the routine analysis of pitch-and-roll buoy wave data. J. Phys. Oceanogr. 18 (7), 1020–1034.

Landwehr, S., Volpi, M., Haumann, F.A., Robinson, C.M., Thurnherr, I., Ferracci, V., Baccarini, A., Thomas, J., Gorodetskaya, I., Tatzelt, C., Henning, S., Modini, R.L., Forrer, H.J., Lin, Y., Cassar, N., Simó, R., Hassler, C., Moallemi, A., Fawcett, S.E., Harris, N., Airs, R., Derkani, M.H., Alberello, A., Toffoli, A., Chen, G., Rodríguez-Ros, P., Zamanillo, M., Cortés-Greus, P., Xue, L., Bolas, C.G., Leonard, K.C., Perez-Cruz, F., Walton, D., Schmale, J., 2021. Exploring the coupled ocean and atmosphere system with a data science approach applied to observations from the antarctic circumnavigation expedition. Earth Syst. Dyn. 12 (4), 1295–1369.

Longuet-Higgins, M.S., 1963. The effect of non-linearities on statistical distributions in the theory of sea waves. J. Fluid Mech. 17 (3), 459–480.

Massom, Robert A., Stammerjohn, Sharon E., 2010. Antarctic sea ice change and variability – physical and ecological implications. Polar Sci. 4 (2), 149–186.

Masson, Diane, LeBlond, P.H., 1989. Spectral evolution of wind-generated surface gravity waves in a dispersed ice field. J. Fluid Mech. 202, 43–81.

Meylan, Michael H., Bennetts, Luke G., Kohout, Alison L., 2014. In situ measurements and analysis of ocean waves in the antarctic marginal ice zone. Geophys. Res. Lett. 41 (14), 5046–5051.

Meylan, M.H., Bennetts, L.G., Mosig, J.E.M., Rogers, W.E., Doble, M.J., Peter, M.A., 2018. Dispersion relations, power laws, and energy loss for waves in the marginal ice zone. J. Geophys. Res.: Oceans 123 (5), 3322–3335.

Meylan, Michael H., Squire, Vernon A., Fox, Colin, 1997. Toward realism in modeling ocean wave behavior in marginal ice zones. J. Geophys. Res.: Oceans 102 (C10), 22981–22991.

Mokus, N.G.A., Montiel, F., 2022. Wave-triggered breakup in the marginal ice zone generates lognormal floe size distributions: a simulation study. Cryosphere 16 (10), 4447–4472.

Montiel, F., Squire, V.A., Doble, M., Thomson, J., Wadhams, P., 2018. Attenuation and directional spreading of ocean waves during a storm event in the autumn beaufort sea marginal ice zone. J. Geophys. Res.: Oceans 123 (8), 5912–5932.

Parkinson, Claire L., 2019. A 40-y record reveals gradual antarctic sea ice increases followed by decreases at rates far exceeding the rates seen in the arctic. Proc. Natl. Acad. Sci. 116 (29), 14414–14423.

Roach, Lettie A., Bitz, Cecilia M., Horvat, Christopher, Dean, Samuel M., 2019. Advances in modeling interactions between sea ice and ocean surface waves. J. Adv. Modelling Earth Syst. 11 (12), 4167–4181.

Shen, Hayley H., Ackley, Stephen F., Yuan, Yong, 2004. Limiting diameter of pancake ice. J. Geophys. Res.: Oceans 109 (C12).

Squire, V.A., 2007. Of ocean waves and sea-ice revisited. Cold Reg. Sci. & Technol. 49 (2), 110–133.

Squire, Vernon A., 2020. Ocean wave interactions with sea ice: A reappraisal. Annu. Rev. Fluid Mech. 52 (1), 37–60.

Squire, Vernon A., Dugan, John P., Wadhams, Peter, Rottier, Philip J., Liu, Antony K., 1995. Of ocean waves and sea ice. Annu. Rev. Fluid Mech. 27 (1), 115–168.

Squire, Vernon A., Moore, Stuart C., 1980. Direct measurement of the attenuation of ocean waves by pack ice. Nature 283.

Sutherland, Peter, Gascard, Jean-Claude, 2016. Airborne remote sensing of ocean wave directional wavenumber spectra in the marginal ice zone. Geophys. Res. Lett. 43 (10), 5151–5159.

Swart, Sebastiaan, Gille, Sarah T., Delille, Bruno, Josey, Simon, Mazloff, Matthew, Newman, Louise, Thompson, Andrew F., Thomson, Jim, Ward, Brian, du Plessis, Marcel D., Kent, Elizabeth C., Girton, James, Gregor, Luke, Heil, Petra, Hyder, Patrick, Pezzi, Luciano Ponzi, de Souza, Ronald Buss, Tamsitt, Veronica, Weller, Robert A., Zappa, Christopher J., 2019. Constraining southern ocean air-sea-ice fluxes through enhanced observations. Front. Marine Sci. 6.

Tersigni, Ippolita, Alberello, Alberto, Messori, Gabriele, Vichi, Marcello, Onorato, Miguel, Toffoli, Alessandro, 2023. High-resolution thermal imaging in the antarctic marginal ice zone: Skin temperature heterogeneity and effects on heat fluxes. Earth Space Sci. 10 (9), e2023EA003078.

Thomson, Jim, 2022. Wave propagation in the marginal ice zone: connections and feedback mechanisms within the air–ice–ocean system. Phil. Trans. R. Soc. A 380 (2235), 20210251.

Vichi, M., 2022. An indicator of sea ice variability for the antarctic marginal ice zone. Cryosphere 16 (10), 4087–4106.

Wadhams, Peter, Squire, Vernon A., Ewing, J.A., Pascal, R.W., 1986. The effect of the marginal ice zone on the directional wave spectrum of the ocean. J. Phys. Oceanogr. 16 (2), 358–376.

Wadhams, Peter, Squire, Vernon A., Goodman, Dougal J., Cowan, Andrew M., Moore, Stuart C., 1988. The attenuation rates of ocean waves in the marginal ice zone. J. Geophys. Res.: Oceans 93 (C6), 6799–6818.

Wahlgren, S., Thomson, J., Biddle, L.C., Swart, S., 2023. Direct observations of wave-sea ice interactions in the antarctic marginal ice zone. J. Geophys. Res.: Oceans 128 (10), e2023JC019948.